

Technical University of Denmark



## Phase Transitions of Materials Studied by Synchrotron Radiation

Forskningscenter Risø, Roskilde

*Publication date:*  
1988

*Document Version*  
Publisher's PDF, also known as Version of record

[Link back to DTU Orbit](#)

*Citation (APA):*  
Buras, B. (1988). Phase Transitions of Materials Studied by Synchrotron Radiation. (Risø-M; No. 2719).

### DTU Library

Technical Information Center of Denmark

---

#### General rights

Copyright and moral rights for the publications made accessible in the public portal are retained by the authors and/or other copyright owners and it is a condition of accessing publications that users recognise and abide by the legal requirements associated with these rights.

- Users may download and print one copy of any publication from the public portal for the purpose of private study or research.
- You may not further distribute the material or use it for any profit-making activity or commercial gain
- You may freely distribute the URL identifying the publication in the public portal

If you believe that this document breaches copyright please contact us providing details, and we will remove access to the work immediately and investigate your claim.

# **Phase transitions of materials studied by synchrotron radiation**

**Lecture notes**

**Bronislaw Buras**

**Phase transitions of materials studied by  
synchrotron radiation**

**Lecture notes**

**Bronislaw Buras**

**Dedicated to Ulrich Bonse on the occasion of his 60th birthday**

**Abstract**

Synchrotron radiation is an excellent tool for studies of structural phase transitions. Among others it enables to follow the transition as a function of the parameter inducing the transition (e.g. pressure, temperature) and time. The latter possibility is due to the short recording times resulting from the high intensity of S.R.

For these studies simultaneous recording of the whole diffraction pattern is of great importance. This is achieved either by using a monochromatic beam and a position sensitive detector (PSD) or by using x-ray energy dispersive diffraction (XED).

The first method is described only briefly because of its analogy to the conventional method. In the XED method one uses a polychromatic "white" incident beam, a fixed scattering angle and an energy dispersive detector. The main characteristics of the method is the simultaneous recording of the whole diffraction pattern and the fixed scattering angle. The XED method is discussed in some detail.

Examples of studies of phase transitions using both methods are briefly described.

October 1988

Risø National Laboratory, DK-4000 Roskilde, Denmark

**Seminar**  
**Synchrotron Radiation: Application in Materials**  
**Santander, Spain, 11-15 July 1988**



**ISBN 87-550-1432-1**

**ISSN 0418-6435**

**Grafisk Service, Risø 1988**

<b>Contents</b>	<b>Page</b>
<b>Preface</b> .....	<b>5</b>
<b>1. Introduction</b> .....	<b>7</b>
<b>2. The monochromatic beam method using a position sensitive detector</b> .....	<b>9</b>
<b>2.1 Linear position sensitive detector</b> .....	<b>9</b>
<b>2.2 Curved position sensitive detector</b> .....	<b>10</b>
<b>2.3. Position sensitive detectors and phase transitions</b> .....	<b>12</b>
<b>3. General information about X-ray energy dispersive diffraction (XED)</b> ...	<b>13</b>
<b>4. The formula for integrated intensity for energy dispersive powder     diffractometry</b> .....	<b>16</b>
<b>5. Corrections to the formula for integrated intensity</b> .....	<b>18</b>
<b>5.1. Polarization factor</b> .....	<b>18</b>
<b>5.2. Attenuation factor</b> .....	<b>19</b>
<b>5.3. Solid state detectors and their quantum efficiency</b> .....	<b>20</b>
<b>6. The XED experimental set-up</b> .....	<b>21</b>
<b>7. Precision of the XED method</b> .....	<b>22</b>
<b>8. Applications</b> .....	<b>25</b>
<b>9. References</b> .....	<b>29</b>

## Preface

The lecture notes discuss diffraction techniques for studies of structural phase transitions using X-rays from electron (positron) storage rings. They do not discuss the nature of these transitions, however, they present briefly some examples of results obtained. It is assumed that the reader is familiar with conventional monochromatic beam diffractometry.

The lecture notes have an introductory character and they are limited to studies of powdered crystals and crystallization of amorphous materials. Due to space limitation, the number of drawings is also limited.

The sections devoted to X-ray energy-dispersive diffraction are partly based on the review "Application of energy dispersive diffraction for characterization of materials under high pressure" by B. Buras and L Gerward to appear in Progress in Crystal Growth and Characterization edited by P. Krishna, Pergamon Press.

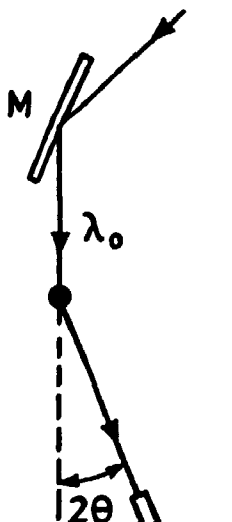
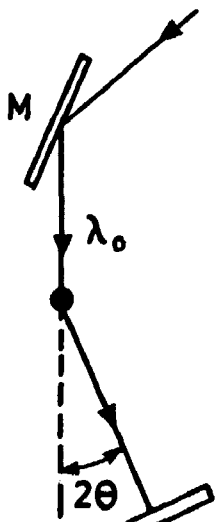
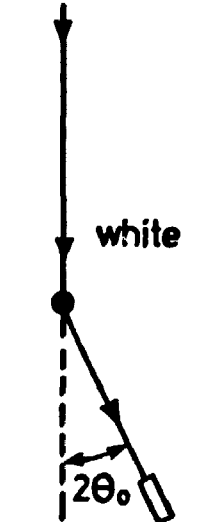
## 1. INTRODUCTION

The X-ray methods used for structural studies of powdered crystals are listed in Table 1 together with a short description of their characteristic features. The Table is self-explanatory, however, some comments might be in place. The wellknown angular scan method with a single counter records the scattered intensity step-by-step as a function of the scattering angle (Scattering vector). This is time-consuming and therefore this method is not suitable for following a phase transition as function of temperature, pressure, time etc. It will not be discussed here.

Fast and simultaneous recording of all reflections is of paramount importance for following the transition of a structure. It can be done using a monochromatic beam and a position sensitive detector or by using a polychromatic ("white") beam and a semiconductor detector. We discuss briefly the first method and in some detail the second one.

Table 1

**X-ray methods for structural studies of powdered crystals  
and amorphous materials.**

Beam incident on the sample	Monochromatic		Polychromatic
Method	Angular scan $\lambda_0 = \text{const.}$		Energy scan $\theta_0 = \text{const.}$
Instrument	Double or triple axis diffractometer	Double axis diffractometer	Energy dispersive diffractometer
Detector	Conventional	Position sensitive	Energy sensitive
Recording of scattered intensity	Step-by-step	Simultaneously	Simultaneously
<p>Experimental set-up (schematically)</p> <p>M-monochromator</p> <p>● Sample collimators not shown</p>	 <p>Proportional counter</p>	 <p>PSD</p>	 <p>SSD</p>



## 2. THE MONOCHROMATIC BEAM METHOD USING A POSITION SENSITIVE DETECTOR (PSD).

### 2.1. Linear position sensitive detector (LPSD).

We recall that a LPSD equipped with a relevant electronics and computing facilities records the position  $x$  at which the scattered photon hits the detector (Fig. 1). For technical details see Ref. 1 and references therein. The  $2\theta_0$  angle corresponding to  $x=0$  is known from the alignment procedure and thus  $x$  defines the scattering angle  $2\theta$ . As a result, a LPSD records simultaneously a diffraction pattern in a range  $\Delta(2\theta) = 2\theta_f - 2\theta_0$ , which depends on the effective length  $l_{eff}$  of the counter and its distance from the sample (see Fig. 1). The detector is usually mounted on the arm of the diffractometer permitting a change of the angle  $2\theta_0$ . This permits the recording of a diffraction pattern in any range of the scattering angle in steps of  $\Delta(2\theta)$  defined above. Usually it is done in a bit smaller steps.

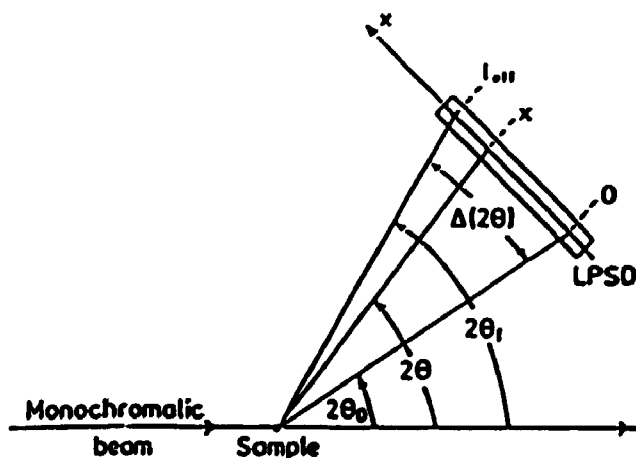


Fig. 1. The geometry of recording the scattered radiation using a linear position sensitive detector (exaggerated).

We illustrate the above general considerations with an example [2]. Fig. 2 shows a part of the diffraction pattern of  $Al_2Y_4O_9$  obtained using a wavelength  $\lambda_0 = 1.391 \text{ \AA}$  from the storage ring DORIS (HASYLAB, Hamburg) and a LPSD. The effective length of the detector was 42.5 mm and it was placed at a distance 902 mm from the powdered sample covering a range of  $\Delta(2\theta)$  equal to  $2.7^\circ$ . The detector had a resolution of 0.05 mm corresponding to 3 milledegree. The detector

was divided into 450 pixels (each corresponding to 6 millidegree), however, for statistical reasons the pixels were added pairwise to give a mean pixel "length" of 12 millidegree. The data were collected in steps of  $1.7^\circ$  in  $2\theta$  and counting times were from one to two minutes for one setting. To cover the same range of  $1.7^\circ$  with a single detector moved in steps equal to the pixel "length" of 12 millidegree would take 140 times longer, for example, about 5 hours instead of 1 minute! It was not possible to reduce further the recording time by increasing the incident intensity because of the maximum count rate accepted by the detector ( $5000 \text{ s}^{-1}$ ). It is the usual limitation when working with PSD's.

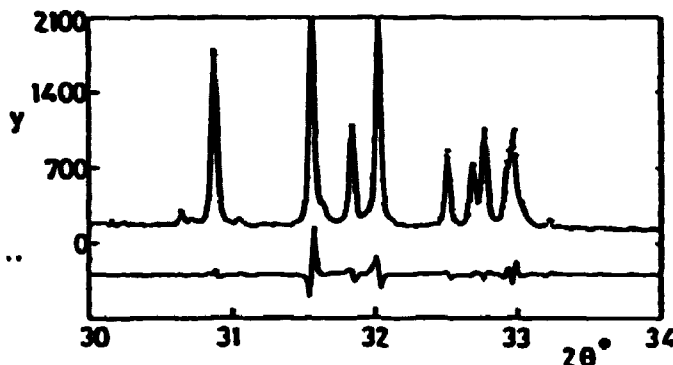
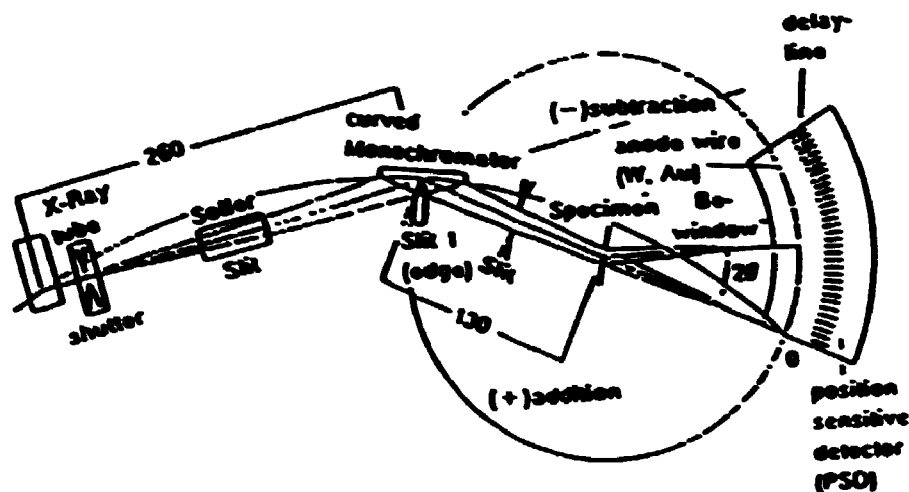


Fig. 2 Diffraction pattern of  $\text{Al}_2\text{Y}_4\text{O}_9$  obtained with SR and a linear PSD. The points are the observations and the continuous line is the calculated profile (after Ref. 2).

## 2.2. Curved PSD.

In use are also curved position sensitive detectors. Fig. 3 shows, as an example, such a set-up at an X-ray tube<sup>\*</sup>[3]. The geometrical details are shown in the figure. The maximum counting rate is  $5 \cdot 10^4$ , thus larger than that of the linear detector described above. However, the resolution is worse - 0.15 mm corresponding in this case to 70 millidegree. At 1.5 kW X-ray tube and a curved graphite or germanium monochromator the measuring thime is usually 2-3 minutes (total  $10^5$ - $10^6$  pulses), and for kinetic studies 0.5-1 minute.

\* ) There are no obvious reasons why such a detector could not be placed at an SR source.



**Fig. 3.** The monochromatic X-ray beam and the curved position of the PSD between 0 and 60° (2θ) on the STOE focusing monochromatic beam diffractometer. Linear dimensions are in mm (After Ref. 3).

Fig. 4 shows the diffraction pattern of medium complexity from monoclinic glucose monohydrate. Fig. 4(a) shows the conventional scintillation detector scan of a 0.5 mm capillary. The step width was 20 millidegree, the step time was 15 s and the presented section was obtained in about 5 h. Two different diagrams obtained with the curved PSD described above are presented. Fig. 4(b) shows the raw data and Fig. 4(c) the smoothed data. The figures show that with a similar resolution and with a statistics only about 25% poorer, the PSD data are obtained in a time about 50 times shorter.

From about 100 indexed powder patterns the author of the paper [3] concludes that the absolute accuracy of the lattice constant given by the conventional method was better than 0.1% and for the curved PSD method better than 0.2%. The latter accuracy could be improved using a linear PSD, which, as we have seen, has a better resolution.

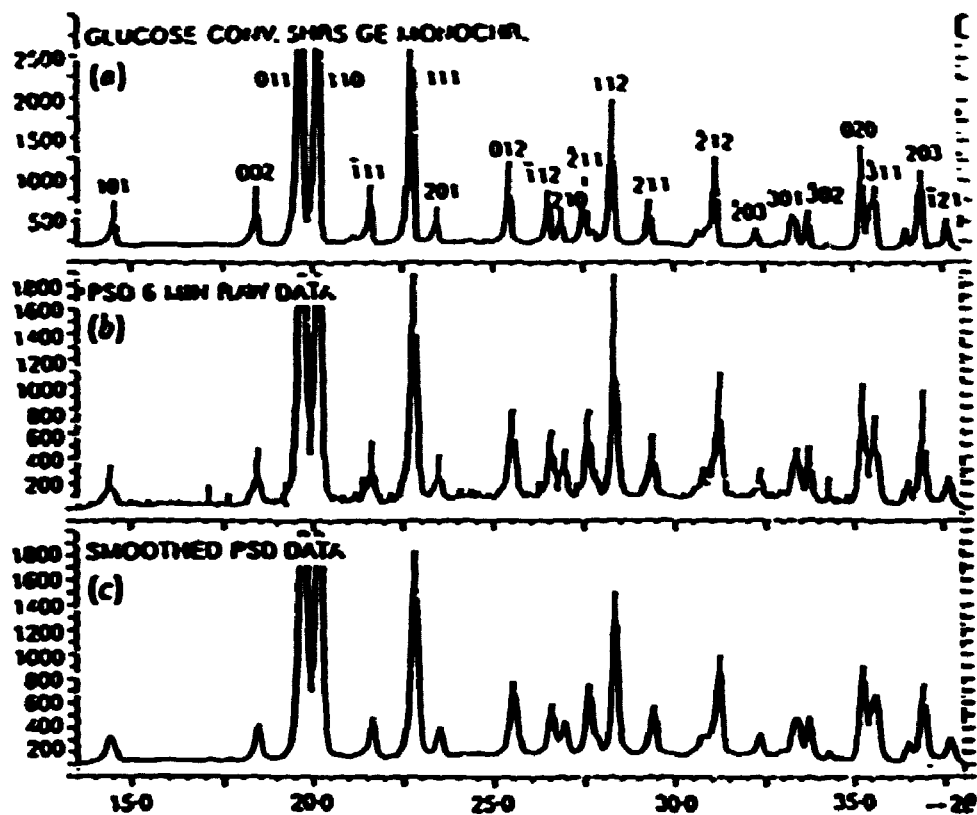
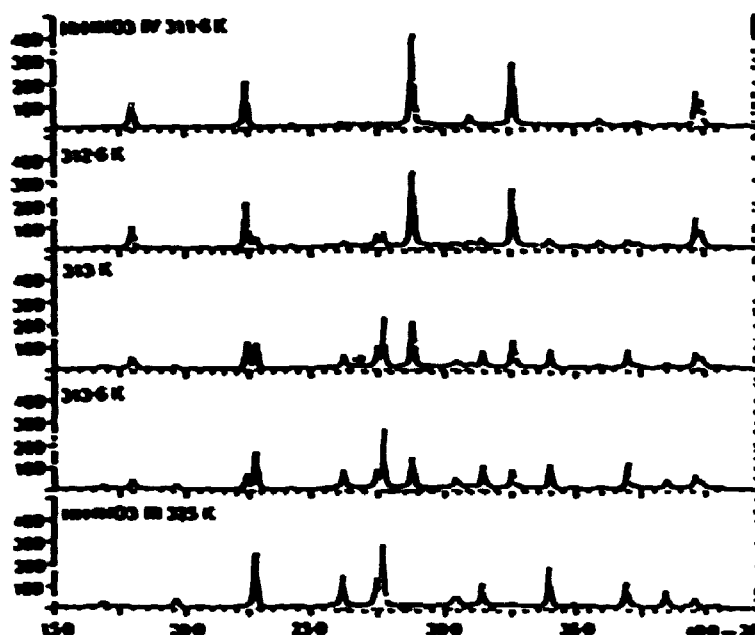


Fig. 4. Conventional and PSD diffraction patterns obtained with  $\text{CuK}\alpha_1$  radiation from a 45 kV tube, 25 mA, Ge monochromator [3]. See also text.

### 2.3. PSD's and phase transitions.

As already mentioned in the introduction, simultaneous recording of all reflections is of paramount importance for following the changes of a structure. The short exposure time plays also an important role, in particular in kinetic studies. As an example Fig. 5 presents PSD data showing the  $\text{NH}_4\text{NO}_3$  phase transition IV to III [3]. One sees that the transition begins at about 313 and is completed at 325.

It follows from the above that PSD's are very suitable for studies of phase transition. They have, however, some disadvantage when the sample is in a special environment (high pressure cell, cryostat, furnace etc.). The PSD method requires a relatively wide window ( $60^\circ$  and more) in the cell keeping the special environment and this is not always simple, in particular, in the case of high pressures. In this case a fixed scattering angle presents a great advantage. The X-ray energy dispersive diffraction method fulfils this requirement and is discussed in the next sections.



**Fig. 5.** PSD raw data showing the  $\text{NH}_4\text{NO}_3$  phase transition IV  $\rightarrow$  III. Time interval between subsequent patterns was 2 mm (1 min exposure time and 1 min pause for data acquisition). (After Ref. 3).

### **3. GENERAL INFORMATION ON X-RAY ENERGY DISPERSIVE DIFFRACTION (XED)**

The method invented in 1968 [4,5]<sup>\*</sup> is primarily applied to crystallographic studies of powdered samples and the following discussion is mainly devoted to this case.

Figure 6 shows the comparison between the angle-dispersive and the energy-dispersive methods. As already mentioned, in the latter one uses a well collimated (the collimators are not shown in the figure) polychromatic ("white") beam and scatters it under a fixed angle  $2\theta_0$  from a powdered sample. The photon energy (wavelength) distribution of the diffracted photons is analyzed by means of a solid state detector (SSD) connected to a multichannel pulse-height analyser.

<sup>\*</sup> An annotated bibliography covering the years 1968-78 can be found in ref. [6].

POWDER DIFFRACTION TECHNIQUES

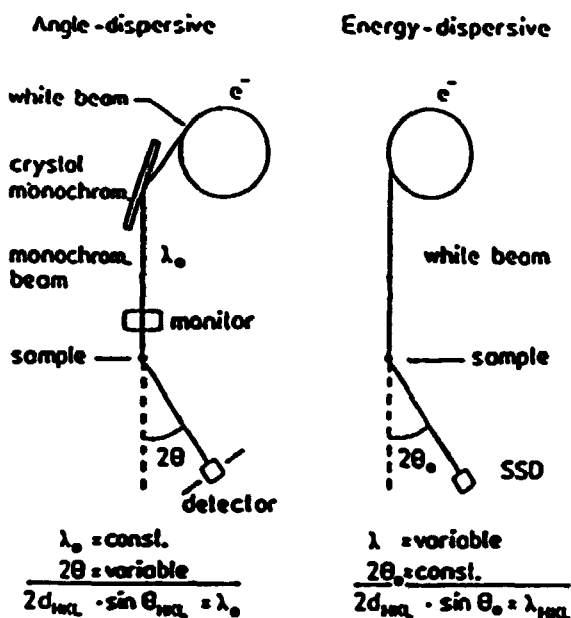


Fig. 6. X-ray powder diffractions techniques using SR.

Each set of crystal lattice planes of the powdered sample of spacing  $d_H$  ( $H$  indicates indices of reflection  $HKL$ ) selects from the incident white spectrum photons of energy  $E_H$  (wavelength  $\lambda_H$ ) fulfilling the Bragg equation

$$2d_H \sin\theta_0 = \lambda_H = \frac{hc}{E_H} = \frac{12.398 \text{ (keV} \cdot \text{Å)}}{E_H} \quad (1a)$$

( $h$  is Planck's constant,  $c$  the velocity of light), and reflects them into the detector. Figure 7 shows an example of a pattern measured at the synchrotron radiation source DORIS (Hasylab, Hamburg, FRG) The Bragg equation is usually written in a more convenient form for XED:

$$d_H \cdot E_H \cdot \sin\theta_0 = C = 6.199 \text{ (keV} \cdot \text{Å)} \quad (1b)$$

The integrated intensity of a reflection recorded by the detector along a unit length of the Debye-Scherrer ring is given by the formula

$$I_H = C [i_0(E) E^{-2} j |F|^2 \cdot \eta(E) A(E, \theta_0) C_p(E, \theta_0)]_H \sin^{-3} \theta_0 \Delta\theta_0 \quad (2)$$

where  $C$  is a constant for a given experiment,  $i_0(E)$  the incident beam intensity per unit energy range,  $j$  the multiplicity factor,  $F$  the structure factor including the atomic scattering factors and the temperature factors,  $\eta(E)$  the detector quantum efficiency,  $A(E, \theta_0)$  the attenuation factor,  $C_p(E, \theta_0)$  the polarization factor and  $\Delta\theta_0$  is a convolution of the incident and diffracted beams divergences. All values in the bracket should be taken for the  $H$  reflection. The formula is derived in Section 4.

From the positions  $E_H$  of the reflections in the energy scale, recorded by the solid state detector (see Fig. 6), and the known scattering angle  $2\theta_0$ , one calculates a set of interplanar spacings  $d_H$  using eq. (1b). From the diffraction

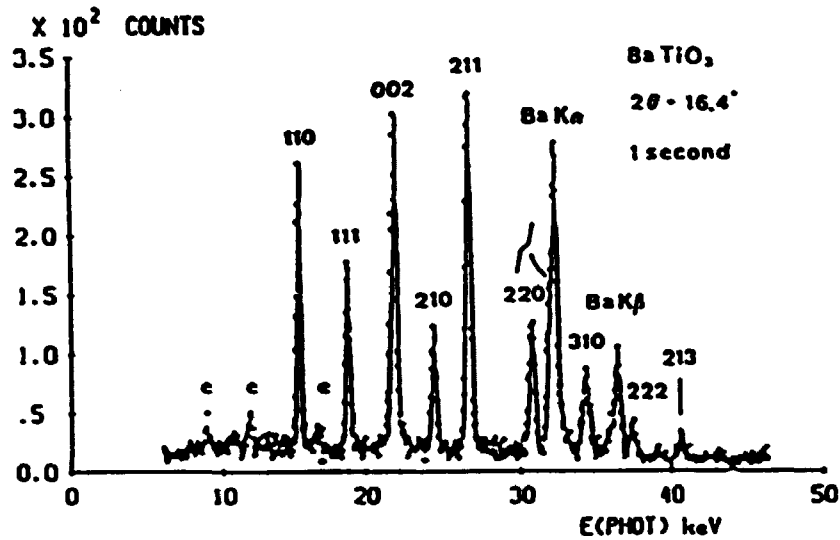


**Fig. 7.** Diffraction pattern from BaTiO<sub>3</sub> powder recorded in 1s at a scattering angle  $2\theta_0 = 16.4^\circ$  at DORIS (3.7 GeV, 14 mA,  $\lambda_c = 1.34 \text{ \AA}$ ) with an ultra pure germanium detector.

pattern, one calculates the integrated intensities  $I_H$ . Then by means of eq. 2 one can calculate a set of structure factors  $[|F|]_H$ , providing that  $[i_0(E), \eta(E), A(E, \theta_0), C_p(E, \theta_0)]_H$  are known. These factors are discussed in Sections 4 and 5.

With a set of interplanar spacings  $d_H$  and a set of structure factors  $[|F|]_H$  one determines the structure of a given sample in the same way as in the case of the angular dispersive method.

The main characteristic features of the energy dispersive method where it differs from the x-ray monochromatic beam (angular scan) method, are the following:

- (a) The incident beam is polychromatic ("white"),
- (b) The scattering angle  $2\theta_0$  is fixed during a measurement but can be optimized for each particular experiment. There is no mechanical movement during the recording.
- (c) The detector is an energy-dispersive one,
- (d) All reflections are recorded simultaneously,
- (e) The counting time is relatively short due to the high detector efficiency and simultaneous recording of reflections.

There are many applications of the method. By far the most important are studies of structural transitions. In this case the simultaneous appearance of all reflections and the short exposure times are essential. The fixed geometry is very convenient when cryostats, ovens or high pressure cells are used (only one inlet and one outlet window are necessary). XED is also very useful for structural studies of amorphous materials and textures.

A white (polychromatic) X-ray beam can be obtained from X-ray tubes (Bremsstrahlung) and from synchrotron radiation (SR) sources. The discussion in the present lecture notes is limited to SR. However, references are also made to experiments using X-ray tubes because each of these experiments could be made also with SR, though the opposite is not always true.

#### 4. THE FORMULA FOR INTEGRATED INTENSITY FOR ENERGY DISPERSIVE POWDER DIFFRACTOMETRY [4,7]

In XED the relation between the integrated intensity and the structure factor is different from the one in the angular dispersive method. The basic formula is derived below within the framework of the kinematical theory of diffraction beginning with the classical formula for the power  $I_H^{cl}$  of a monochromatic beam of wavelength  $\lambda_0$  diffracted by a non-absorbing powder sample [7]. For the basic formula it is assumed also that the efficiency of the detector is 1. All corrections are included later. For the whole Debye-Scherrer ring we have

$$I_H^{cl} = r_o^2 i_o(\lambda) \Delta\lambda \frac{\lambda^3 \cdot j_H |F_H|^2}{4 \sin \theta_B} C_p(E, \theta_B) \frac{\delta V}{V^2} \quad (3)$$

where  $r_o$  is the classical electron radius,  $\delta V$  the sample volume,  $V$  the unit cell volume,  $\theta_B$  is the Bragg angle and  $\Delta\lambda$  the spectral width of the incident monochromatic radiation. The meaning of the other symbols was already explained in Section 1. The reason we write the polarization factor as  $C_p(E, \theta_B)$  and not  $(1 + \cos^2 2\theta_0)/2$  as we do in the angular dispersive method, will become clear in Section 4.1. It should be noted that  $i_o(\lambda) \Delta\lambda$  is the intensity of the incident beam usually denoted by  $I_o$  in the angular dispersive methods. In the latter ones  $\Delta\lambda$  is defined either by the spectral width of the characteristic line or by the spectral width of the monochromatic beam obtained by means of a single crystal monochromator. In the white beam energy dispersive method  $\Delta\lambda$  depends on the overall divergence  $\Delta\theta_o$  of the incident and diffracted beams. By differentiation of the Bragg equation

$$2d \sin \theta = \lambda \quad (4)$$

with  $d$  constant one obtains

$$\Delta\lambda = \lambda \cdot \cos \theta \cdot \Delta\theta \quad (5)$$

and the formula for the integrated intensity in the white beam energy dispersive method for powdered crystals is

$$I_H^o = r_o^2 \left[ i_o(\lambda) \cdot \lambda^4 |F|^2 \cdot C_p(E, \theta_o) \right]_{11} \frac{\cos \theta_o \cdot \Delta\theta_o \delta V}{4 \sin^2 \theta_o V^2} \quad (6)$$



for the whole Debye-Scherrer ring. All values in the bracket are taken for the H reflection.

If the detector of length  $\ell$  (along the Debye-Scherrer ring) is located at distance R from the sample then the measured integrated intensity is  $\ell/(2\pi R \sin 2\theta_0)$  times smaller and thus

$$I_H^o = \frac{r_o^2 \cdot \ell}{16\pi R} \left[ i_o(\lambda) \lambda^4 \cdot |F|^2 \cdot C_p(E, \theta_0) \right]_H \sin^{-3} \theta_0 \frac{\delta V}{V^2} \Delta \theta_0 \quad (7)$$

As mentioned in Section 3, the diffracted intensity is recorded as a function of photon energy. It is therefore convenient to express the integrated intensity in terms of the photon energy, which is related to the wavelength by the wellknown expression

$$E = \frac{hc}{\lambda} \quad (8)$$

The incident beam intensity per unit wavelength range,  $i_o(\lambda)$ , is related to the intensity per unit energy range,  $i_o(E)$ , through

$$i_o(\lambda) = i_o(E) \left| \frac{dE}{d\lambda} \right| = i_o(E) \frac{E^2}{hc} \quad (9)$$

From eqs. (7), (8) and (9) one has

$$I_H^o = C_o [i_o(E) E^{-2}] |F|^2 \cdot C_p(E, \theta_0) \sin^{-3} \theta_0 \Delta \theta_0 \quad (10)$$

where  $C_o = (hc)^3 r_o \cdot \ell \cdot \delta V / (16\pi R V^2)$  is constant for a given experiment.

In order to obtain the full formula one must multiply  $I_H^o$  with a detector efficiency factor  $\eta(E)$  and an attenuation factor  $A(E, \theta_0)$ . Finally one gets

$$I_H = C_o [i_o(E) E^{-2}] |F|^2 \eta(E) A(E, \theta_0) C_p(E, \theta_0) \sin^{-3} \theta_0 \Delta \theta_0 \quad (11)$$

For a given experimental set-up both  $\theta_0$  and  $\Delta \theta_0$  are constants and can be included into the constant  $C_o$ . One obtains

$$I_H = C [i_o(E) E^{-2}] |F|^2 \cdot \eta(E) A(E, \theta_0) C_p(E, \theta_0) \quad (12)$$

with

$$C = C_o \sin^{-3} \theta_0 \cdot \Delta \theta_0, \quad (13)$$

It follows from the formula (12) that calculations of the structure factors from the measured integrated intensities require the knowledge of the spectral distribution  $i_o(E)$  of the incident beam. In the case of SR the spectrum  $i_o(E)$  can be calculated in the first approximation from the storage ring parameters taking into account the attenuation of the beam by all materials which it penetrates on its way between the source and the sample. It can also be inferred from a diffraction pattern of a known sample.

## 5. CORRECTIONS TO THE FORMULA FOR INTEGRATED INTENSITY

### 5.1. Polarization factor [8]

The polarization factor  $C_p(E, \theta_0)$  depends obviously on the polarization of the incident beam,  $P(E)$ , which is known to depend on the photon energy  $E$ .  $P(E)$  is defined with respect to a given plane as

$$P(E) = [i_{o,p}(E) - i_{o,n}(E)] / [i_{o,p}(E) + i_{o,n}(E)] \quad (14)$$

where  $i_{o,p}(E)$  and  $i_{o,n}(E)$  are the parallel and normal components of the incident beam intensity with respect to this plane.

When dealing with synchrotron radiation, the polarization  $P(E)$  is usually defined with respect to the plane of the electron orbit which is horizontal. Synchrotron radiation emitted by electrons on an ideal orbit is fully polarized, with the polarization vector in the plane of the electron orbit. In the case of a non-ideal electron orbit, the usual case, the radiation is not fully polarized in the orbital plane. However, the polarization  $P(E)$  can be calculated in the first approximation from the parameters of the storage ring. For more precise knowledge of the polarization it should be measured (see e.g. ref. 9).

For an incident non-polarized beam, the polarization factor, as is well known, equals

$$C_p = \frac{1 + \cos^2 2\theta_0}{2} \quad (15)$$

For an incident beam with a degree of polarization  $P(E)$  the polarization factor in the kinematical approximation equals

$$C_p(E, \theta_0) = \frac{1}{2} [1 + \cos^2 2\theta_0 - P(E) \cos 2\alpha \cdot \sin^2 2\theta_0] \quad (16)$$

where  $\alpha$  is the angle between the plane defined by the incident and diffracted beam directions and the plane with respect to which the polarization  $P(E)$  was defined. In the case of synchrotron radiation the latter plane is horizontal and thus for scattering in this plane  $\alpha = 0$  and

$$C_p(E, \theta_0) (\text{horizontal}) = \frac{1}{2} [1 + \cos^2 2\theta_0 - P(E) \sin^2 2\theta_0] \quad (17)$$

and for scattering in the vertical plane  $\alpha = 90^\circ$  and

$$C_p(E, \theta_0) (\text{vertical}) = \frac{1}{2} [1 + \cos^2 2\theta_0 + P(E) \sin^2 2\theta_0] \quad (18)$$

As mentioned above in the case of a storage ring  $P(E)$  can be calculated and thus also  $C_p(E, \theta_0)$ . When no great precision is required one can assume that  $P(E) \approx 1$  and thus

$$C_p(E, \theta_0)(\text{horizontal}) \approx \cos^2 2\theta_0 \quad (19)$$

$$C_p(E, \theta_0)(\text{vertical}) \approx 1 \quad (20)$$

As shown in Fig. 8 there exists in the case of a horizontal scattering plane a "blind" region around  $2\theta = 90^\circ$ . A vertical scattering plane is much more favourable because for all energies and all scattering angles  $C_p(E, \theta_0)(\text{vertical}) \approx 1$ . However, the mechanical construction of the diffractometer, mounting of furnaces, cryogenic equipment etc. are easier to handle when X-rays are scattered in the horizontal plane.

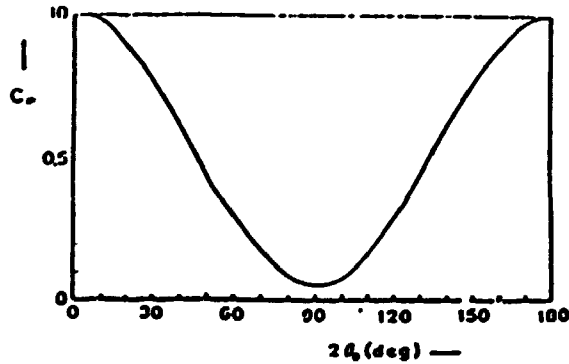


Fig. 8. The polarization factor  $C_p(E, \theta_c)$  for a powdered sample calculated for a horizontal scattering plane and an ideal electron orbit.

## 5.2. Attenuation factor $A(E, \theta_0)$ in XED.

Well established methods and formulas exist for calculating the attenuation factor for the monochromatic beam angular dispersive method. In the energy-dispersive method the photon energy (wavelength) changes from reflection to reflection and thus one calculates the attenuation factor separately for each reflection using the above mentioned methods and formulas. As a consequence, the attenuation factor is a function both of photon energy and scattering angle. Attention should be called to the dramatic changes of absorption in the vicinity of an absorption edge. In the calculations one can use within a good approximation the photon energy corresponding to the peak position.

### 5.3. Solid state detectors; detector efficiency [10].

The detectors usually used are high purity Germanium (HPGe) and Si(Li). The Lithium drifted detectors must be kept at liquid nitrogen temperature all the time. The extra pure Ge detector must be at liquid nitrogen temperature only during the measurements. The detectors have a build-in low noise preamplifier kept at the same temperature as the detector. The preamplifier is connected to a multichannel pulse height analyzer through an amplifier. The data can be displayed on a fluorescent screen and recorded on magnetic tape and with an X-Y plotter. They can also be directly transferred to the memory of a computer for data treatment.

There are two important characteristics of semiconductor detectors: (i) energy resolution and (ii) quantum efficiency  $\eta(E)$ . The energy resolution is discussed in Section 7. The efficiencies are illustrated in Fig. 9. One sees that the Si(Li) detector has a quantum efficiency of unity for low energy photons, but drops rapidly for photons above 30 keV. It should be noted also that the efficiency curve is a smooth one. In the case of a Ge detector, the high efficiency extends to higher photon energies. However, the efficiency curve in this case has a kink at 11.1 keV due to the absorption K-edge in Germanium. As a consequence, it is difficult to

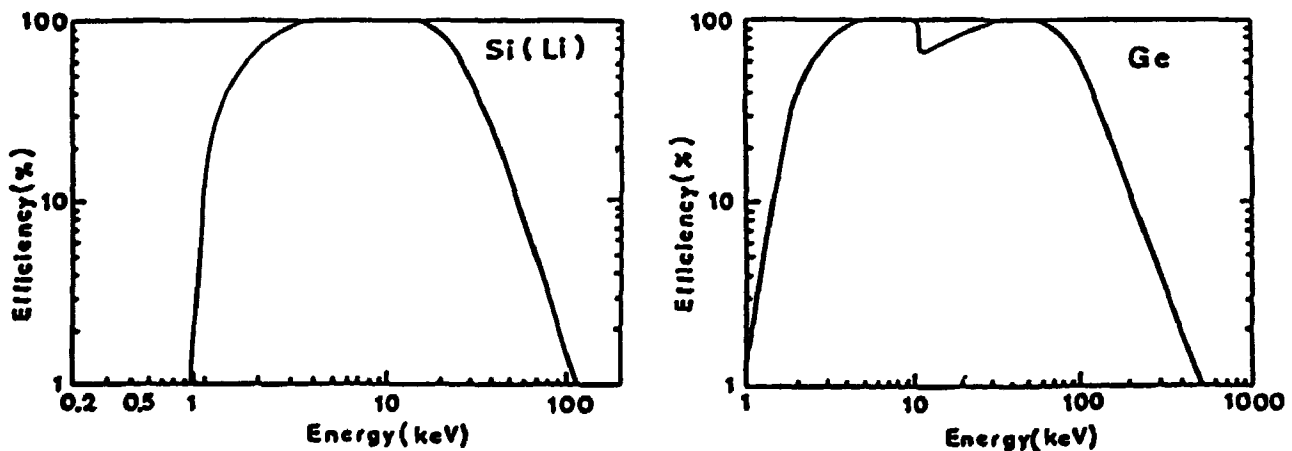


Fig. 9. Quantum efficiency of semiconductor detectors as function of photon energy.

estimate the spectral distribution  $i_0(E)$  in the region of about 11 keV. For reasons of both high efficiency and smoothness of the efficiency curve the Si(Li) detector is used for low energy photons, say, up to 30 keV and Ge detectors for high energy photons above  $\sim 12$  keV.

## 6. XED EXPERIMENTAL SET-UP [7-9]

The principal elements of an experimental set up were already shown in Fig. 6. More details of a set-up at a SR source are shown in Fig. 10. (Examples of existing XED diffractometers are among others described in Refs. 11-13). The directions and divergences of the incident and diffracted beams are defined by slits  $S_1$ ,  $S_2$  and  $S_3$ ,  $S_4$ , respectively. They also define the mean scattering angle  $2\theta_0$ .

The divergences of the incident and diffracted beams depend on the slit widths and the source-sample and sample-detector distances, respectively.

The source-sample distance depends on the storage ring and the location of the experiment in the experimental hall. It varies, say, from 10 m to 40 m. The sample-detector distance is much smaller, usually below 1 m. As a consequence, the slit widths for the diffracted beam must be much smaller than for the incident beam.

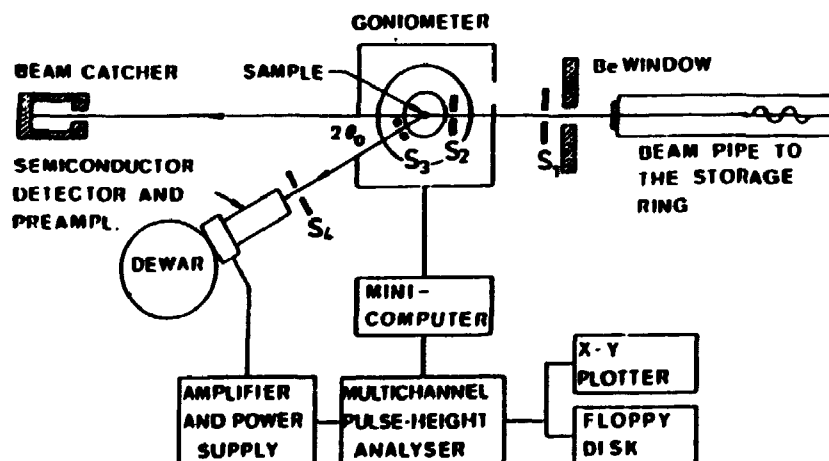


Fig. 10. An XED set-up at a SR source (schematically).

The dimensions of the source in a storage ring varies from several millimeters to parts of a millimeter. Table 2 presents, as examples, the FWHM's of the dimensions of S.R. sources from bending magnets of DORIS and the expected ones of the ESRF.

Table 2

Full widths at half maximum of S.R. sources (in mm)

	DORIS	ESRF expected
Horizontal plane	2.4	0.4
Vertical plane	0.7	0.3

Due to these small source sizes, the slit 1 is in many cases superfluous<sup>\*)</sup>. Assume, for example, a source size of 1 mm, the width of slit S<sub>2</sub> equals 0.2 mm and the source-sample distance is 20 m. Then the divergence of the incident beam is 10<sup>-4</sup> radians. For the diffracted beam it is difficult to obtain such a small divergence. Even for 1 m distance between the sample and the detector and slits S<sub>3</sub> and S<sub>4</sub> of widths 0.1 mm each, one obtains a divergence of 2·10<sup>-4</sup> radians. At present S.R. sources this may lead to insufficient intensity. At the ESRF it should not involve any problems.

In view of the above it is clear that one does not need the divergence of the incident beam better than 10<sup>-4</sup> radians. Thus the slit S<sub>1</sub> is in general superfluous. For small samples (e.g. in a diamond envil cell) the slit S<sub>3</sub> could also be omitted.

The recording time depends clearly on the number of photons per second passing the solid angle defined by the source size and slit S<sub>2</sub>. Thus the figure of merit of an SR source for XED is brightness.

In order to reduce the background appropriate shielding must be used. In case of S.R. for safety reasons the whole experimental set-up is placed in a hutch covered with lead (~5 mm thick). Thus all movements of the detector, sample and goniometer must be remotely controlled. An important element of the set-up is a beam catcher (see Fig. 10) reducing substantially the background.

## 7. PRECISION OF THE XED METHOD

By differentiation of the Bragg equation 1b and under the assumption that errors  $\delta E$  and  $\delta\theta_0$  of the measurements of photon energy and Bragg angle, respectively, are of a statistical nature, one obtains

$$\frac{\delta d}{d} = \left[ \left( \frac{\delta E}{E} \right)^2 + \left( \cot\theta_0 \delta\theta_0 \right)^2 \right]^{1/2} \quad (21)$$

where  $\delta d$  is the absolute precision of the interplanar spacing measurement.

$\delta\theta_0$  is usually 5 millidegree  $\approx 10^{-4}$  radians or smaller. As we shall see later,  $\theta_0$  is seldom smaller than 5° and thus  $\cot\theta_0 \delta\theta_0$  is usually smaller than 10<sup>-3</sup>.

---

<sup>\*)</sup> One should use, however, a diaphragm in order to reduce the background.

In order to calculate  $\delta E$  it is necessary to consider two values: the energy resolution  $\delta E_D$  of the detector system and  $\delta E_\theta$ , the energy broadening of the reflection due to beam divergence. Following Ref. 14 we have

$$\delta E_D = [(\Delta E_{amp})^2 + 5.546 F \cdot \epsilon E]^2 \quad (22)$$

where  $\Delta E_{amp}$  is due to the dark current through the SSD and to the noise in the field-effect transistor and the preamplifier,  $F$  is the Fano factor,  $\epsilon$  is the energy required for creating an electron-hole pair.  $\delta E_\theta$  we get by differentiating the Bragg equation with  $d = \text{const}$

$$\delta E_\theta = -E \cot \theta_0 \Delta \theta_0 \quad (23)$$

where  $\Delta \theta_0$  is the beam divergence. Assuming a Gaussian distribution for both  $\delta E_D$  and  $\delta E_\theta$  one obtains

$$\delta E = [(\delta E_D)^2 + (\delta E_\theta)^2]^{1/2} \quad (24)$$

Simple algebra gives

$$\frac{\delta E}{E} = C^{-1} [(\Delta E_{amp} \cdot d \cdot \sin \theta_0)^2 + 5.546 C F \epsilon d \sin \theta_0 + (C \cot \theta_0 \Delta \theta_0)^2]^{1/2} \quad (25)$$

with  $C = 6.199 \text{ keV \AA}$ .

Fig. 11 shows examples of the dependence of  $\delta E/E$  on  $\theta_0$  for two interplanar spacings  $0.5 \text{ \AA}$  and  $1 \text{ \AA}$  and two divergences  $10^{-4}$  and  $10^{-3}$  radians. Note that in

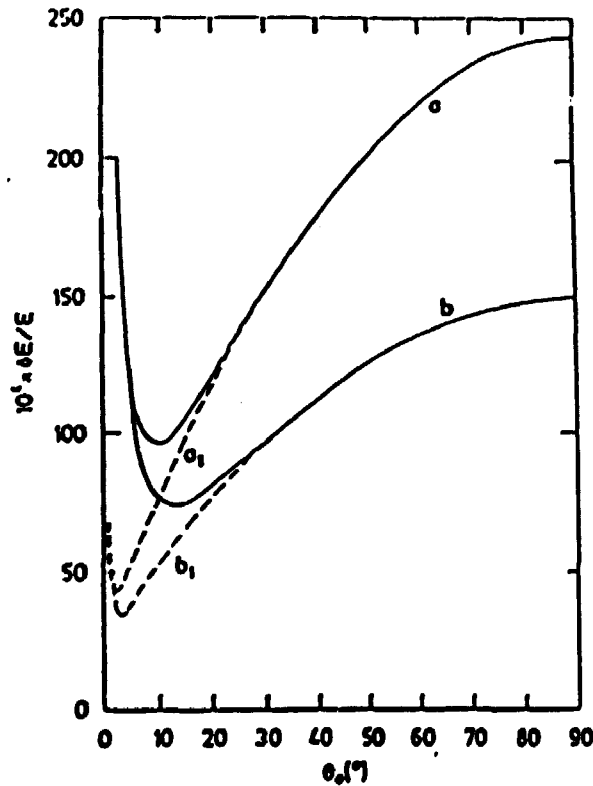


Fig. 11.  $\delta E/E$  as function of  $\theta_0$  for two interplanar spacings:  $1 \text{ \AA}$  (curve a) and  $0.5 \text{ \AA}$  (curve b). The full lines are for  $\Delta \theta_0 = 10^{-3}$ , the dotted for  $\Delta \theta_0 = 10^{-4}$ .

all four cases  $\delta E/E$  decreases with decreasing  $\theta_0$  down to a certain minimum and then increases rapidly. The initial decrease is due to the first term in Eq. 25, however, when  $\theta_0$  becomes very small the leading term is the last one, which blows up for small  $\theta_0$ . Fig. 6 illustrates also that  $\delta E/E$  decreases with decreasing interplanar spacing, and that the minimum value of  $\delta E/E$  is smaller for smaller  $d$  and shifts to smaller  $\theta_0$ . A small  $\theta_0$  for a given lattice spacing means a large photon energy.

It follows from Fig. 11 that for  $\Delta\theta_0 = 10^{-4}$  radians - possible to achieve with SR - and angles, say, smaller than  $15^\circ$  (but not too small)  $\delta E/E$  is smaller than  $10^{-2}$ . It should be, however, recalled that  $\delta E$  is the full width at half maximum and the centroid of the reflection can be measured with a precision, say, 10 times or more better. Thus the  $\delta E/E$  value in Eq. 21 can be made smaller than  $10^{-3}$  and thus of the same order as  $\cot\theta_0\delta\theta_0$ . In conclusion,  $\delta d/d$  can be measured with a precision of  $10^{-3}$  or better. It should also be noted that the relative values of the interplanar spacings can be measured with a still better precision because for  $\theta_0$  constant  $\delta d/d = \delta E/E$  and the second term in Eq. 23 drops out.

Fig. 12 shows an example of an improvement of energy resolving power by increasing the photon energy. One easily notices that although  $\delta E$  increases with

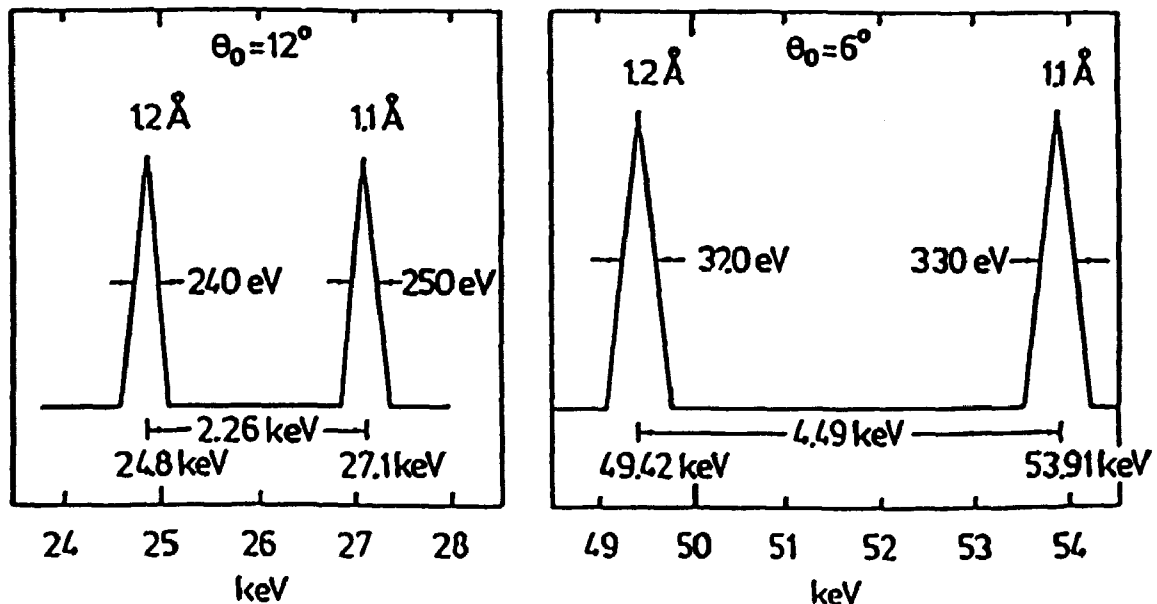


Fig. 12. An example of an improvement of energy resolving power by decreasing the scattering angle.

photon energy, the distance between the reflections increases faster and they are better separated.

In conclusion one sees that high energy photons improve both the accuracy of lattice spacing measurements and the resolving power.



To get an idea of the required photon energies we assume  $\Delta\theta_0 = 10^{-4}$  and  $\theta_0 = 5$  which is close to the value of  $\theta_0$  leading to small  $\delta E/E$  for  $d = 0.5 \text{ \AA}$ . In this case  $E = 142 \text{ keV}$ . Wavelength shifters can easily emit photons of this energy, however the efficiency of the Ge solid state detector decreases several times (see Fig. 9). Due to the high intensity of modern S.R. sources, this should not cause any problems in most cases one can think of.

The accuracy of structure factor determination depends - in addition to accuracy with which  $E$  can be measured - on the accuracy with which the incident intensity and the attenuation, polarization and detector efficiency factors (see Eq. 2) can be estimated. Also, the energy dependent Compton effect should be taken into account. All these lead in praxis to the conclusion that in general the XED is a less precise method for structure determination than the monochromatic beam angular method. However, it is very useful for identification of known structures, for example, appearing in course of a phase transition. Its other qualities enumerated in Section 3 make the XED a useful and convenient method in many cases. Some examples are briefly described in the section 8.

## 8. APPLICATIONS

### 8.1. Introduction

The XED found many applications in material sciences, however, the main interest lies in two broad areas. The first involves structural studies and phase transformations at high pressures and high (low) temperatures. The second involves structural studies of amorphous materials including crystallization phenomena. However, one can find also applications of XED in other fields, as for example, studies of texture in thin films [15,16], anharmonicity [17], measurements of mean-square atom displacements [18], and others. Some of the applications use X-ray tubes, some SR. In the present chapter we quote both because any experiment performed with an X-ray tube can be performed also, and with better results, at a SR source, however, the opposite is not always the case.

### 8.2. Structural studies at high pressures [15-18]

Structural studies of solids under high (tens and hundreds of kilobars) and very high (megabars) pressures have become in recent years increasingly important for basic and applied solid state physics and geophysics [19]. The high and very high static pressures are obtained by means of diamond-anvil cells DAC (see Ref. 20) and the most frequently used diffraction method is XED.

Fig. 13 shows the principle of a DAC cell. The sample is placed in a small hole in a 0.1-0.3 mm thick metal foil (gasket). The pressure is exerted by the two flat diamond faces pressed against each other. The volume of the sample is very small ( $10^{-5}$ - $10^{-3}$  mm<sup>3</sup>) and thus for structural studies a high brightness X-ray source is needed. A SR source fulfils this requirement. The DAC is placed on the sample table of an XED diffractometer mentioned in Section 5 and described in some detail in Ref. 11-13.

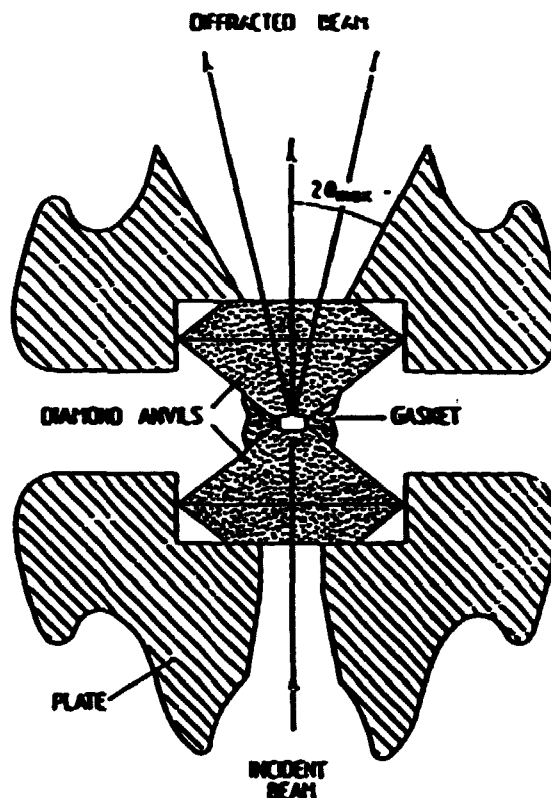


Fig. 13. The diamond anvil high pressure cell (schematically).

As an example of such studies we discussed the pressure induced transformation of  $\text{YbH}_2$  at room temperature [21]. The structure of this material at atmospheric pressure is orthorhombic. The XED diffraction patterns at four different pressures are presented in Fig. 14. It is clearly seen that at 14.3 GPa (143 kbar) some new reflections appear in addition to those characterizing the orthorhombic structure. At 17.0 GPa the reflections from the orthorhombic structure have partly disappeared, and at 28.2 GPa they are absent. On the basis of the measured interplanar spacings the high pressure structure was identified as hexagonal. The orthorhombic phase can be viewed as a distorted hexagonal packing with  $c/a \approx 1.6$ , and the transformation as a collapse to a hexagonal structure with  $c/a = 1.34$ .

This example illustrates clearly the ability of studies of phase transformation in situ, recording the transformation step by step with changing pressure.

Another example illustrates structure studies at ultra-high pressures [22]. XED and SR were used to study rhenium up to 2.16 Mbar (216 GPa). It was found that the HCP structure exists up to this pressure (volume fraction  $v/v_0 = 0.734$ ) and the  $c/a$  ratio is independent of pressure. In this study the X-rays were also used to obtain a pressure profile across the diamond face. This required a very narrow beam of a very high intensity.

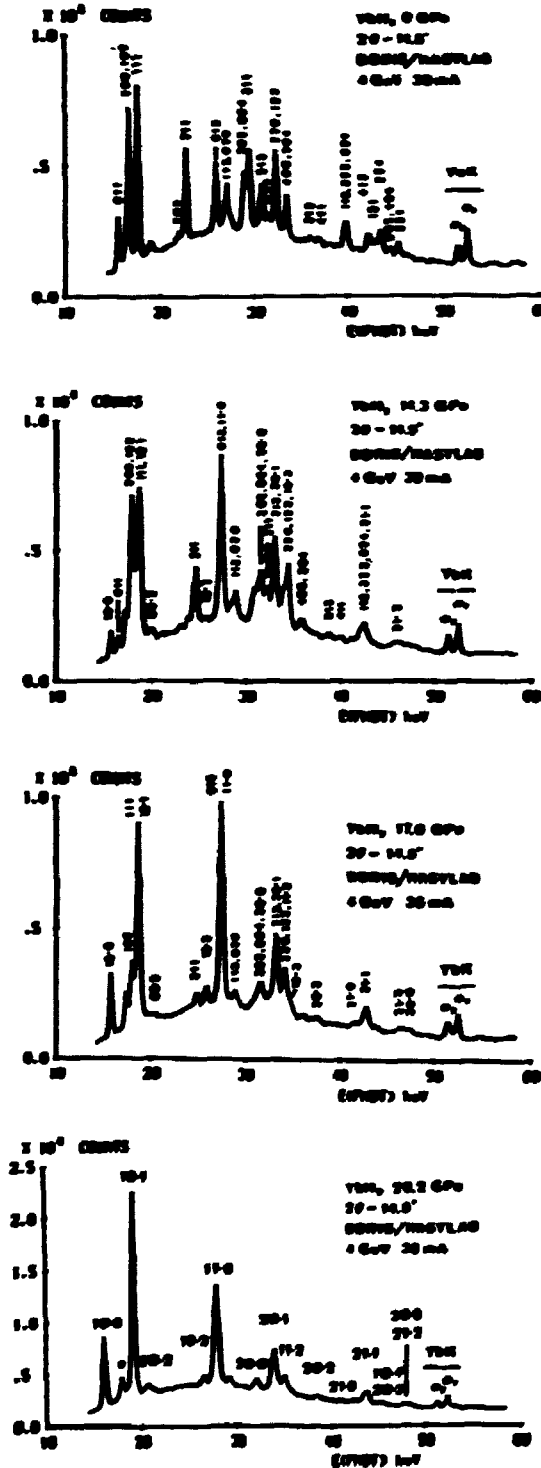


Fig. 14. XED pattern of  $\text{YbH}_2$  at several pressures (after Ref. 17).

### 8.3. Crystallization of metallic glasses.

Metallic glasses have attracted much interest due to their remarkable magnetic and mechanical properties. Because the amorphous state is metastable it can be transformed to a crystalline one by annealing at elevated temperatures. These studies are interesting from a scientific point of view and are also important for practical applications of metallic glasses. As an example, we briefly present the work on crystallization of Fe-Si-B [23]. Amorphous ribbons of  $Fe_{90-x}Si_xB_{10}$  with  $x$  ranging from 7 to 21 were investigated using XED and S.R. at DORIS at HasyLab/DESY. The samples were placed in a special furnace and could be heated up to several hundred degrees C. The annealing was isothermal. The temperature was raised to the desired value and then the structural changes as a function of time were studied by means of XED. The counting time was several minutes. Then the temperature was raised and again the structural changes were measured as a function of time. Fig. 15 shows an example of a diffraction pattern obtained. By analysing the patterns it was possible to study the time dependence of the evolving new phase and identify its crystallographic structure. The latter was done mainly by examination of the peaks positions and comparing the interplanar spacings found in this way with the ones of known chemical compounds of iron, silicon and beryllium.

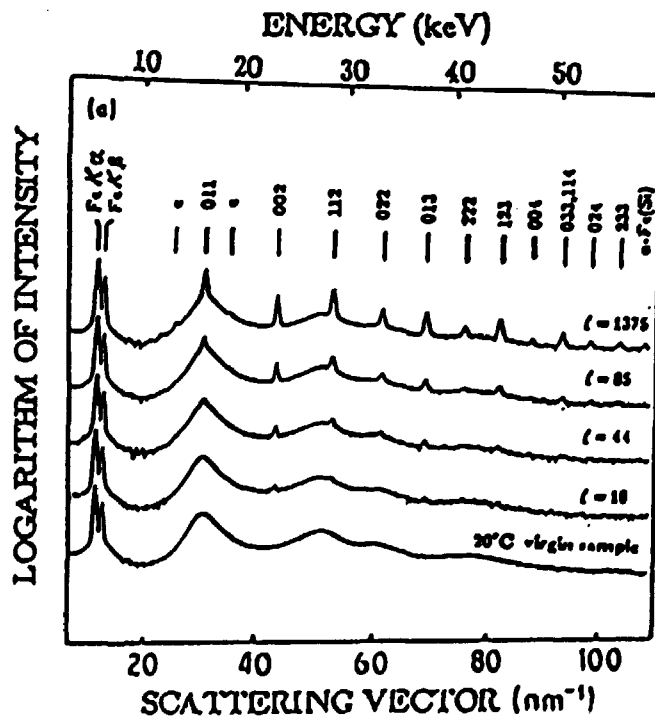


Fig. 15. Series of diffraction patterns of the crystallization of  $Fe_{83}Si_7B_{10}$  after annealing at  $350^\circ C$  for 18, 44, 85 and 1375 minutes. The pattern of the virgin amorphous sample at room temperature is also shown (after Ref. 23).

## REFERENCES

1. Gabriel, A., Dauvergne, F. and Rosenbaum, G. (1978). Linear, circular and two-dimensional position sensitive detectors. *Nucl. Instr. and Methods* **152**, 191-194 and references therein.
2. Lehmann, M.S., Nørlund Christensen, A., Fjellvåg, H., Feidenhans'l, R. and Nielsen, M. (1987). Structure determination by use of pattern decomposition and the Rietveld method on synchrotron X-ray and neutron powder data; the structure of  $\text{Al}_2\text{Y}_4\text{O}_9$  and I2O4. *J. Appl. Cryst.* **20**, 123-129.
3. Wölfel, E.R. A novel curved position sensitive proportional counter for X-ray diffractometry (1983). *A. Appl. Cryst.* **16**, 341-348.
4. Buras, B., Chwaszczewska, J., and Szmid, Z. (1968). Fixed angle scattering (FAS) method for x-ray crystal structure analysis. Institute of Nuclear Research, Warsaw, Report No. 894/II/PS, 10 pp.
5. Giessen, B.C. and Gordon, G.E. (1968). X-ray diffraction: New high-speed technique based on x-ray spectroscopy. *Science* **159**, 973-975.
6. Laine, E. and Lahteenmaki, I. (1980). The energy dispersive x-ray diffraction method: annotated bibliography 1968-1978. *J. Mater. Sci.* **15**, 296.
7. Buras, B. and Gerward, L. (1975). Relations between integrated intensities in crystal diffraction methods for x-rays and neutrons. *Acta Cryst.* **A31**, 372-374, and references therein.
8. Olsen, J. Staun, Buras, B., Jensen, T., Alstrup, O., Gerward, L. and Selsmark, B. (1978). Influence of polarization of the incident beam on integrated intensities in x-ray energy-dispersive diffractometry. *Acta Cryst.* **A34**, 84-87.
9. Templeton, D.H. and Templeton, L.K. (1988). Polarization of synchrotron radiation. *Appl. Cryst.* **21**, 151-153.

10. Worgan, J.S. (1982). Energy dispersive detectors for synchrotron radiation. Nucl. Instrum. Methods 201, 85-91.
11. Olsen, J. Staun, Buras, B., Gerward, L. and Steenstrup, S. (1981). A spectrometer for x-ray energy-dispersive diffraction using synchrotron radiation. J. Phys. E: Scient. Instrum. 14, 1154-1158.
12. Skelton, E.F., Qadri, S.B., Webb, A.W., Lee, C.W. and Kirkland, J.P. (1983). Improved system for energy-dispersive x-ray diffraction with synchrotron radiation. Rev. Sci. Instruments 54, 403-409.
13. Brister, K.E., Vohra, Y.K. and Ruoff, A.L. (1986). Microcollimated energy-dispersive x-ray diffraction apparatus for studies at megabar pressures with a synchrotron source. Rev. Sci. Instrum. 57, 2550-2563.
14. Buras, B., Niimura, N. and Olsen, J. Staun (1978). Optimum resolution in x-ray energy dispersive diffractometry. J. Appl. Cryst. 11, 137-140 and references therein.
15. Hariuchi, T., Fukao, K., Matsushige, K. (1987). New evaluation method of evaporated organic thin films by energy dispersive x-ray diffractometer. Jpn. J. Appl. Phys. 26, L 1839-41.
16. Hart, M. Parish, W., Masciocchi, N. (1987). Studies of texture in thin films using synchrotron radiation and energy dispersive diffraction. App. Phys. Lett. (USA) 50, 897-9.
17. Tranguda, J.M., Trautman, C., Heald, S.M. (1987). X-ray diffraction study of anharmonicity in V<sub>3</sub>Si. Phys. Rev. B 35, 4193-8.
18. Metzger, T.H. (1986). An energy-dispersive x-ray diffraction study of mean-square atom displacements in highly oriented pyrolytic graphite. J. Appl. Cryst. 19, 200-1.
19. Skelton, E.F. (1984). High pressure research with synchrotron radiation. Physics Today, September 44-52.

20. Minomura, S. (editor). (1985). Solid State Physics under Pressure. Recent Advance with Anvil Devices. D. Reidel Publishing Company, Dordrecht.
21. Olsen, J.S., Buras, B., Gerward, L., Johansson, B., Lebech, B., Skriver, H. and Steenstrup, S. (1984). A new high-pressure phase and the equation of state of YbH<sub>2</sub>. Physica Scripta 29, 503-507.
22. Vohra, Y.K. Duclos, S.J. Ruoff, A.L. (1987). High pressure x-ray diffraction studies on rhenium up to 216 GPa (2.16 Mbar). Phys. Rev. B 36, 9790-2.
23. Minor, W., Schönfeld, B., Lebech, B., Buras, B. and Dmowski, W. (1987). Crystallization of Fe-Si-B metallic glasses studies by X-ray synchrotron radiation. J. Mater. Sci. 22, 4144.

<b>Title and author(s)</b>  <b>Phase transitions of materials studied by synchrotron radiation</b>  <b>Lecture notes</b>  <b>Bronislaw Buras</b>	<b>Date</b> <b>October 1988</b>
	<b>Department or group</b>  <b>Physics</b>
	<b>Groups own registration number(s)</b>
	<b>Project/contract no.</b>
<b>Pages</b> <b>34</b> <b>Tables</b> <b>2</b> <b>Illustrations</b> <b>15</b> <b>Reference</b> <b>23</b>	<b>ISBN</b> <b>87-550-1432-1</b>
<b>Abstract (Max. 2000 char.)</b> <p>Synchrotron radiation is an excellent tool for studies of structural phase transitions. Among others it enables to follow the transition as a function of the parameter inducing the transition (e.g. pressure, temperature) and time. The latter possibility is due to the short recording times resulting from the high intensity of S.R.</p> <p>For these studies simultaneous recording of the whole diffraction pattern is of great importance. This is achieved either by using a monochromatic beam and a position sensitive detector (PSD) or by using x-ray energy dispersive diffraction (XED).</p> <p>The first method is described only briefly because of its analogy to the conventional method. In the XED method one uses a polychromatic "white" incident beam, a fixed scattering angle and an energy dispersive detector. The main characteristics of the method is the simultaneous recording of the whole diffraction pattern and the fixed scattering angle. The XED method is discussed in some detail.</p> <p>Examples of studies of phase transitions using both methods are briefly described.</p>	
<b>Descriptors</b>	
<p>Available on request from Rise Library, Rise National Laboratory, (Rise Bibliotek, Forskningscenter Rise), P.O. Box 48, DK-4000 Roskilde, Denmark.  Telephone 02 37 12 12, ext. 2302. Telex: 49116, Telefax: 02 35 05 00</p>	



**Available on exchange from:  
Risø Library,  
Risø National Laboratory,  
P.O. Box 49, DK-4000 Roskilde, Denmark  
Phone (02) 37 12 12 ext. 2262**

**ISBN 87-550-1432-1  
ISSN 0418-6435**